Laboratory Investigation (2021) 101:26–37
https://doi.org/10.1038/s41374-020-00484-3

ARTICLE

A MXI1-NUTM1 fusion protein with MYC-like activity suggests a novel oncogenic mechanism in a subset of *NUTM1*-rearranged tumors

Christopher R. McEvoy[1] · Holly Holliday[2,3] · Niko Thio[4] · Catherine Mitchell[1] · David Y. Choong[1] · Bhargavi Yellapu[1,5] · Hui San Leong[1] · Huiling Xu[1] · Stephen Lade[1] · Judy Browning[1] · Elena A. Takano[1] · David J. Byrne[1] · Anthony J. Gill[6,7,8] · Cuong P. Duong[9] · Jason Li[4] · Andrew P. Fellowes[1] · Stephen B. Fox[1,10] · Alexander Swarbrick[2,3] · Owen W. J. Prall[1]

Received: 15 June 2020 / Revised: 10 August 2020 / Accepted: 17 August 2020 / Published online: 1 September 2020

Abstract

Most *NUTM1*-rearranged neoplasms (NRNs) have fusions between *NUTM1* and *BRD* (bromodomain-containing) family members and are termed NUT carcinomas (NCs) because they show some squamous differentiation. However, some NRNs are associated with fusions between *NUTM1* and members of the *MAD* (MAX dimerization) gene family of MYC antagonists. Here we describe a small round cell malignancy from the gastro-esophageal junction with a previously unreported fusion between *NUTM1* and the *MAD* family member *MXI1*. In contrast to NCs, the *MXI1-NUTM1* tumor did not show squamous differentiation and did not express *MYC, TP63* or *SOX2*, genes known to be targets of BRD-NUTM1 proteins and critical for NC oncogenesis. Transcriptome analysis showed paradoxical enrichment of MYC target genes in the *MXI1-NUTM1* tumor despite the lack of *MYC* expression. When expressed in vitro MXI1-NUTM1 partially phenocopied MYC, enhancing cell proliferation and cooperating with oncogenic HRAS to produce anchorage-independent cell growth. These data provide evidence that MAD family members, which are normally repressors of MYC activity, can be converted into MYC-like mimics by fusion to NUTM1. The pathological features and novel oncogenic mechanism of the *MXI1-NUTM1* tumor show that identification of *NUTM1* fusion partners can be important for accurate diagnostic classification of some NRN subtypes, and potentially may guide therapeutic options.

Introduction

Solid malignancies associated with structural variants involving nuclear protein in testis member 1 (*NUTM1* or *NUT*) are a rare and under-recognized group of tumors. Originally they were identified as an extremely aggressive subset of poorly differentiated squamous cell carcinomas,

Supplementary information The online version of this article (https://doi.org/10.1038/s41374-020-00484-3) contains supplementary material, which is available to authorized users.

✉ Owen W. J. Prall
owen.prall@petermac.org

1 Department of Pathology, Peter MacCallum Cancer Centre, Melbourne, VIC 3000, Australia

2 The Kinghorn Cancer Centre, Garvan Institute of Medical Research, Darlinghurst, NSW 2010, Australia

3 Faculty of Medicine, St Vincent's Clinical School, UNSW Sydney, Sydney, NSW 2010, Australia

4 Cancer Research Division, Peter MacCallum Cancer Centre, Melbourne, VIC 3000, Australia

5 Epworth Healthcare, Melbourne, VIC, Australia

6 Cancer Diagnosis and Pathology Group, Kolling Institute of Medical Research, Royal North Shore Hospital, St Leonards, NSW 2065, Australia

7 NSW Health Pathology, Department of Anatomical Pathology, Royal North Shore Hospital, Sydney, NSW 2065, Australia

8 University of Sydney, Sydney, NSW 2065, Australia

9 Division of Cancer Surgery, Peter MacCallum Cancer Centre, Melbourne, VIC 3000, Australia

10 University of Melbourne, Parkville, VIC 3010, Australia

termed NUT carcinomas (NC), predominantly located in the midline of the head, neck, and mediastinum, and refractory to chemotherapy [1]. In NCs *NUTM1* is fused to the genes for bromodomain (BRD)-containing chromatin-interacting proteins *BRD4* (70–80% of cases) or *BRD3* (10%), or genes for BRD-associated proteins including *NSD3*, *ZNF532*, and *ZNF59* in another 10% of cases [1]. However, the identification of tumors with novel *NUTM1* fusion partners has expanded the morphologic and genetic spectrum of *NUTM1*-rearranged neoplasms (NRNs) [reviewed in [2]]. Some NRNs have small round blue, spindle, rhabdoid and/or plasmacytoid cell morphology, lack evidence of squamous or epithelial differentiation, and are probably best classified as sarcomas [3]. One class of these sarcoma or sarcoma-like NRNs harbors *NUTM1* fusions to members of the MAX Dimerization (*MAD*) gene family [3–8].

Here we describe a small round cell gastroesophageal junction malignancy harboring a novel fusion between *NUTM1* and *MXI1* (also known as *MXD2*), a member of the *MAD* family of MYC antagonists. We present in vivo and in vitro evidence to support a fundamentally different oncogenic mechanism for *MXI1-NUTM1* when compared to a typical NC-associated fusion, *BRD3-NUTM1*. We discuss the implications of our findings to the diagnosis, clinical course and treatment of NRNs.

Materials and methods

Targeted RNA sequencing

Tumor RNA was extracted from FFPE slides using the AllPrep DNA/RNA FFPE kit (Qiagen, Hilden, Germany). Targeted fusion analysis was performed using Anchored Multiplex PCR (AMP™) [9] with the Archer FusionPlex™ Oncology Research Panel (ArcherDx, Boulder, CO). cDNA libraries were prepared and sequenced on a MiSeq sequencer (Illumina, San Diego, CA) as per the manufacturer's recommendations. FASTQ files were processed using ArcherDx analysis software to annotate gene fusions and variants (http://analysis.archerdx.com/). For RT-PCR and Sanger sequencing, cDNA was synthesized from RNA using the SuperScript™ VILO™ cDNA Synthesis Kit (Invitrogen, Carlsbad, CA). PCR was performed using AmpliTaq Gold (ThermoFisher Scientific) with priming sites located in *MXI1* exon 5 (5′-GCTCGAGAATTTGGAACGAG-3′) and *NUTM1* exon 3 (5′-CTGGTGGGTCAGAAGTTGGT-3′). PCR product was analyzed on a 2% agarose gel and purified with ExoSAP-IT (ThermoFisher Scientific). Sequencing reactions were performed using the BigDye Terminator v3.1 Cycle Sequencing Kit (ThermoFisher Scientific) and sequencing was conducted on a 3730xl DNA Analyzer (Applied Biosystems, Foster City, CA). Sequencing results were analyzed using Mutation Surveyor software (SoftGenetics, State College, PA). TruSight RNA Fusion and TruSight RNA Pan-Cancer Panel (Illumina, San Diego, CA) cDNA libraries were both prepared and sequenced with a MiSeq sequencer (Illumina, San Diego, CA) as per the manufacturer's recommendations. FASTQ files were analyzed with the RNA-Seq Alignment application on the BaseSpace Sequence Hub (Illumina, San Diego, CA).

Targeted DNA sequencing

Targeted sequencing comprised the analysis of 2.34 Mb genomic regions implicated in cancer, including sequencing of the entire coding regions of 386 genes as well as selected intronic regions (including *NUTM1*) of genes known to be involved in oncogenic fusions. KAPA Hyper (Roche) libraries were prepared and target enriched using SureSelect^{XT} hybridization (Agilent) [10]. Pooled libraries were sequenced at 500× mean coverage on an Illumina NextSeq sequencer (Illumina, San Diego, CA, USA) using paired 75 bp reads. Variants were detected using combined VarScan [11], Mutect [12], and ugSomatic [13] variant callers. Copy number variations were detected using CNspector [14].

Immunohistochemistry

Diagnostic immunohistochemistry (IHC) was performed on sections from FFPE primary tumor tissues as well as on cell blocks of in vitro cultured cells (see below). See Supplementary material for full methods.

Transcriptome analysis by RNA sequencing (RNAseq)

RNA was extracted from FFPE tissue as described above. cDNA libraries were prepared using the NEBNext® Ultra™ II RNA Library Prep Kit (NEB, Ipswich, Mass) with ribodepletion and random priming. Libraries were sequenced on an Illumina NextSeq sequencer (Illumina, San Diego, CA, USA) using paired 75 bp reads. Adapter sequences, primers, and too-short-read sequences were removed using Cutadapt v1.9.1 [15]. Reads were subsequently aligned to human reference genome hg19 using the HISAT2 v2.0.4 read-mapping algorithm [16] and HTSEQ v0.11.2 [17] for gene expression quantification. Data normalization was performed using Voom-limma R package [18]. Reads were subsequently aligned to human reference genome hg19 using the HISAT2 v2.0.4 read-mapping algorithm and gene abundance was quantified using HTSEQ v0.11.2. Library size normalization on the samples was performed using the TMM method [18]. *MXI1-NUTM1* and *BRD3-NUTM1* fusions were detected using JAFFA [19] and Arriba [20].

Gene set enrichment analysis was performed using GSEA [21] preranked mode, using Hallmark MSigDB gene sets. Single sample enrichment analysis were run using ranking based on transcript abundance quantification calculated Salmon [22] which accounts for transcript length bias. Comparative enrichment analysis were run using ranking based on log fold-change of the compared samples.

In vitro cells expressing MXI1-NUTM1 or MYC

MXI1-NUTM1 nucleotide sequences were synthesized and ligated into pcDNA3.1(+)-N-HA by GenScript Ltd (Hong Kong). Retrovirus vectors were constructed for *HA-MXI1-NUTM1*, *MYC* and human oncogenic *HRAS* (encoding HRAS with a glycine to valine substitution at amino acid 12 [23]). NIH-3T3 cells were maintained in DMEM (Gibco) + 10% FBS (HyClone). For retroviral transductions 2.5×10^5 NIH-3T3 mouse fibroblasts were seeded into 6 cm dishes. The following day they were infected with either pMSCVneo empty vector (EV), pMSCVneo *HA-MXI1-NUTM1* or pMSCVpuro *MYC* diluted 1:5 in NIH-3T3 media with 8 µg/mL polybrene (Sigma-Aldrich). Some cells were simultaneously infected with pMSCV *HRAS-IRES-GFP*. Cells were re-infected the following day then put under selection with 800 µg/mL geneticin (Thermo Fisher Scientific) or 1.5 µg/mL puromycin (Sigma-Aldrich) for 1 week. Oncogenic HRAS-positive cells were selected by isolation of GFP-positive cells with a BD FACS Aria III and BD FACS DIVA software.

Immunoblotting

Cells were lysed in RIPA buffer (50 mM Tris-HCl pH 7.4, 1% NP-40, 0.5% sodium deoxycholate, 0.1% SDS, 1% glycerol, 137.5 mM NaCl) and quantified using the Pierce BCA Protein Assay Kit (Thermo Fisher Scientific) according to the manufacturer's instructions. Protein lysates (20–30 µg) were prepared with NuPage loading buffer and reducing agent (Life Technologies) and denatured by heating at 85 °C for 5 min. Samples were loaded onto 4–12% Bis/Tris or 3-8% Tris-Acetate gels (Life Technologies) and run using MOPS or Tris-Acetate running buffers (Life Technologies). Protein was transferred to PVDF membrane (Merck Millipore) using BioRad transfer modules. Membranes were blocked in blocking buffer (LiCOR) for 1 h at room temperature. Primary antibody diluted in 5% BSA/TBS was added to the membranes over night at 4 °C. Antibodies used were HA-Tag (1:1000, CST #3724), MYC (1:1000, Epitomics #1472), HRAS (1:2000, Merck #05-516) and β-actin (1:1000, Sigma-Aldrich #A5441). Fluorescent secondary antibody conjugated to IRDye680 or IRDye800 (LiCOR) diluted in Odyssey blocking buffer (1:15,000–1:20,000) were used for detection. An Odyssey CLx Infrared Imaging System (LiCOR) was used to image the immunoblots.

Cell Titer Glo assay

Cells were seeded into white-walled 96-well plates with 2000 cells per well in 100 µL media with either 1 or 10% FBS. Blank wells with no cells were included to determine background luminescence. Cells were allowed to attach for 4 h, and then baseline measurements were determined using the CellTiter-Glo luminescent assay (Promega) as per the manufacturer's instructions. Briefly, 100 µL CellTiter-Glo buffer was added to each well, plates were placed on an orbital shaker for 2 min, then incubated for 10 min at room temperature protected from the light. Luminescent readings were obtained using a FLUOstar Omega microplate reader (BMG Labtech). Background luminescence values were subtracted from each well. Measurements were taken in the same way 2, 4, and 5 days later and results were expressed as a fold-change relative to day 0.

Incucyte confluence and colony formation assay

NIH-3T3 cells were seeded in 24-well plates with 12,000 cells per well in 1 mL media in duplicate or triplicate. Cells were imaged using an IncyCyte ZOOM live cell imager (zoom40061, Essen BioScience) over a period of 6 days. Images over nine fields of view per well were acquired every 4 h. Phase images were used for calculating cell confluency for EV, MXI1-NUTM1, and MYC cells. GFP images at end point were used for calculating the number of colonies in EV + HRAS, MXI1-NUTM1 + HRAS, and MYC + HRAS transfected cells over five replicate experiments. The average colony counts for each of the transformants from each replicate was used for statistical analysis.

Soft agar colony formation assay

The soft agar colony formation assay was performed as previously described [24]. Briefly, wells of a 12-well plate were coated with 1 mL 0.5% agarose (Lonza Bioscience, Basel) in NIH-3T3 media. Gels were allowed to solidify for 30 min at room temperature, following which 1 mL of a single cell suspension of NIH-3T3 cells at a density of 1000 cells/mL in media containing 0.3% agarose was added. Once set, 500 µL of NIH-3T3 media was added to the wells and plates were incubated at 37 °C, 5% CO_2. Fresh media was added to the wells every 2–3 days for 12 days. Colonies were fixed and stained in 0.1% crystal violet solution (Sigma-Aldrich) containing 10% ethanol for 15 min at room temperature. Gels were de-stained by rinsing five times in distilled water for 5 min each. Colonies were imaged using

a Leica MZ12 dissecting microscope connected to a Leica DFC420C camera using LAS software. Colonies were quantified using FIJI image analysis software [25]. The number of colonies, average colony area, and total colony area was determined for 19 (EV + HRAS) or 18 (MXI1-NUTM1 + HRAS and MYC + HRAS) wells over six (EV + HRAS and MXI1-NUT + HRAS) or 5 (MYC + HRAS) replicate experiments.

Results

Clinical course

A 51-year-old woman, a previous smoker, presented with progressive dysphagia and weight loss. On endoscopy she was found to have a stricture of the lower esophagus and abnormal mucosa extending to the distal stomach. Biopsies showed infiltration of the lamina propria of the esophagus by undifferentiated small cells that expressed NUTM1 by IHC. Staging computed tomography, FDG-PET, and laparoscopy demonstrated a bulky tumor of the distal esophagus, gastroesophageal junction, and lesser curvature of stomach. Nodal, peritoneal, or distant metastases were not identified. The patient underwent an Ivor Lewis esophagectomy with total gastrectomy, colonic interposition, and Roux-en-Y jejunal reconstruction. The patient had a prolonged hospital admission due to post-operative complications. The patient was not eligible for clinical trials and was too unwell to receive chemotherapy, radiotherapy, or any specific targeted therapies. She died 7 months post-surgery from disease progression.

Tumor morphology

Gross examination of the resected specimen showed a near-circumferential tumor centered in the stomach and extending directly into the distal esophagus, a total length of 197 mm (Fig. 1a, b). It had a fleshy, cream-tan cut surface, undermined the normal mucosa and infiltrated the full thickness of the esophageal and gastric walls. Sections (Fig. 1c–e) showed that the tumor formed nests, sheets and strands of discohesive, monotonous, small to intermediate sized cells associated with a small amount of myxoid stroma. Tumor cells had ovoid nuclei with vesicular chromatin, single small but prominent nucleoli, and a small to moderate amount of eosinophilic cytoplasm, some with a vague rhabdoid appearance. There were occasional mitotic figures (2/10 hpf) and apoptotic bodies, as well as extensive lymphovascular, perineural, and intraneural invasion. It somewhat resembled the morphology of a *NUT* carcinoma. However, no squamous or other epithelial differentiation was seen (Fig. 1f). Metastatic tumor was present in multiple para-esophageal, lesser curve, greater curve, and subcarinal lymph nodes.

RNA and DNA sequencing of the *MXI1-NUTM1* tumor

Anchored Multiplex PCR detected chimeric transcripts involving *MXI1* exon 5 (NM_005962.4) fused to *NUTM1* exon 3 (NM_175741.2). These were in frame, and were confirmed by RT-PCR/Sanger sequencing (Fig. 2a) and RNAseq (Fig. 2b, see below). The fusion was subsequently also identified by Illumina TruSight RNA Fusion and RNA Pan-Cancer Panel analysis (not shown). The MXI1-NUTM1 fusion protein was predicted to possess the basic region/helix-loop-helix/leucine zipper domain of MXI1, which mediates its heterodimerization with MAX and sequence specific DNA-binding, as well as the acidic domain (AD1) of NUTM1 that is capable of binding and activating the histone acetyltransferase (HAT) p300 [26]. Other variants detected are shown in Supplementary materials.

Protein expression comparison of the *MXI1-NUTM1* tumor and a *BRD3-NUTM1* NC

Characterization of the *MXI1-NUTM1* tumor by IHC showed nuclear expression of NUTM1 similar to that in a NC with a *BRD3-NUTM1* fusion (Fig. 3). A "speckled" intra-nuclear pattern noted by others in NCs [5, 27] and thought to represent hyperacetylated chromatin "mega-domains" was not observed in either tumor by IHC or immunofluorescence (not shown). The *MXI1-NUTM1* tumor also showed FLI-1 expression in most cells, focally CD99 membrane staining, and weak patchy NSE expression (not shown). It was negative for almost all cytokeratins tested (AE1/AE3, CK5/6, 34betaE12, and CK7), as well as EMA and BerEP4, all of which were robustly expressed in the *BRD3-NUTM1* NC. The low molecular weight cytokeratin marker CAM5.2 also strongly stained the *BRD3-NUTM1* NC but only showed focal faint expression in the *MXI1-NUTM1* tumor. p40 (ΔNp63) is a marker of squamous differentiation, and both *MYC* and *TP63* are key transcriptional targets of BRD-NUTM1 fusion proteins [28, 29]. Notably, the *MXI1-NUTM1* tumor cells showed no staining for MYC or p40. These were both readily detectable in the squamous cells in overlying esophageal epithelium, and in the *BRD3-NUTM1* NC. *SOX2* has also been shown to play a major role in *BRD4-NUTM1*-associated oncogenesis [30]. SOX2 protein was expressed in the *BRD3-NUTM1* NC, but not in the *MXI1-NUTM1* tumor. The results of other immunohistochemistry stains are discussed in Supplementary materials.

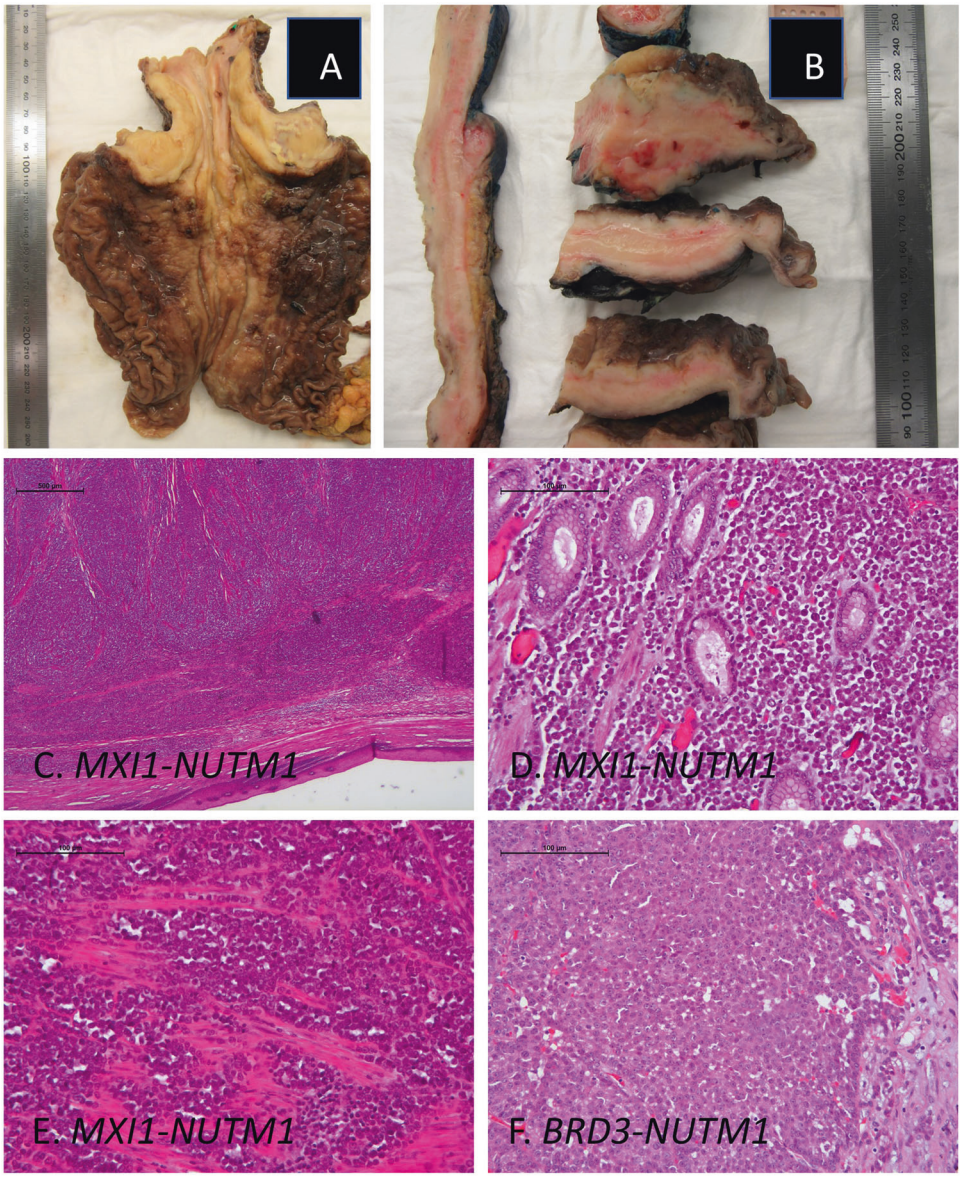

Fig. 1 Tumor morphology. Macroscopic photographs of the esophagectomy specimen from the *MXI1-NUTM1* tumor with the mucosal (**a** opened longitudinally, proximal at the top of image) and cut (**b**) surfaces showing diffuse wall thickening. The serosa is inked black. H&E stained sections from the *MXI1-NUTM1* tumor showing tumor cells invading the esophageal (**c** squamous mucosa at bottom of image) and gastric (**d**, **e**) walls. Note the tumor infiltrating around benign gastric glands (**d**) and invading the muscularis propria (**e**) **f** H&E stained section from a *BRD3-NUTM1* carcinoma. Note the similar morphology to the *MXI1-NUTM1* tumor (compare with **d**, **e**).

Transcriptome comparison of the *MXI1-NUTM1* tumor with a *BRD3-NUTM1* NC

RNAseq confirmed expression of genes directly involved in the oncogenic fusions (*BRD3*, *MXI1*, and *NUTM1*) (Fig. 4a) as well as chimeric *MXI1-NUTM1* and *BRD3-NUTM1* transcripts in the respective tumors. Expression of multiple high and low molecular weight keratins were detected in the *BRD3-NUTM1* NC (Fig. 4a) and in benign esophageal squamous epithelium adjacent to the *MXI1-NUTM1* tumor (not shown). In contrast, only expression of low molecular weight cytokeratins KRT8 and KRT18 were detected in a sample of the *MXI1-NUTM1* tumor that was macrodissected away from esophagogastric epithelium, with low levels of the high molecular weight keratin KRT10. Whilst we cannot dismiss that some of these transcripts were from mesothelium, this was consistent with the weak staining for CAM5.2 by IHC in *MXI1-NUTM1* tumor cells, as this clone reacts with KRT8. RNAseq confirmed that the key NC drivers *MYC*, *TP63*, and *SOX2* were highly expressed in the *BRD3-NUTM1* NC, but showed negligible expression in the *MXI1-NUTM1* tumor, consistent with the IHC results (Fig. 4a). Other transcriptional changes are documented in Supplementary materials.

The *MXI1-NUTM1* tumor has a "MYC-like" transcription signature in the absence of MYC

For BRD-NUTM1 fusion proteins the oncogenic mechanism is thought to involve a "feed-forward" process that results from the histone binding activity of BRD and the histone acetyltransferase activity of the NUTM1-binding

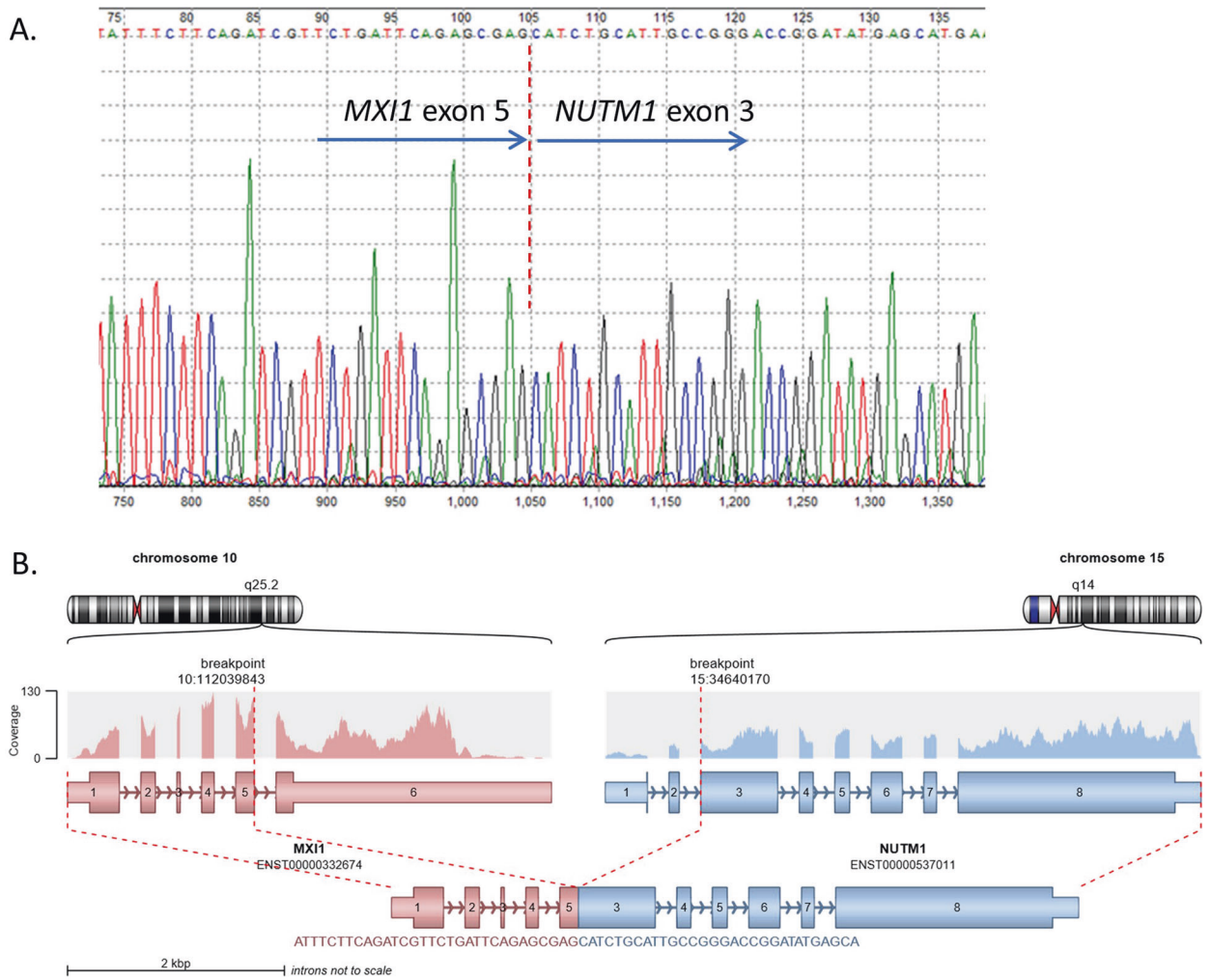

Fig. 2 Identification of the *MXI1-NUTM1* fusion. *MXI1-NUTM1* fusion between *MXI1* exon 5 (NM_005962.4) and *NUTM1* exon 3 (NM_175741.2) confirmed by **a** Sanger sequencing of the RT-PCR product, and **b** RNA whole transcriptome analysis.

protein p300. Binding of BRD-NUTM1 to acetylated histones localized at pro-proliferation genes leads to a cycle of further histone acetylation and BRD-NUTM1 binding. This process sequesters p300 away from pro-differentiation genes, resulting in their hypoacetylation [31]. The net effect is histone hyperacetylation and increased transcription of pro-proliferation genes, and silencing of pro-differentiation genes. However, since MAD-NUTM1 fusions have no known interaction with BRD complexes we have previously hypothesized that they are unlikely to exert their oncogenic effects through this feed-forward mechanism. Instead we have suggested that MAD-NUTM1 fusions will dimerize with MAX through the MAX-interacting domain of the MAD partner, and that these heterodimers would bind to E-boxes near MYC target genes and upregulate gene expression. This model predicts that increased expression of MYC target genes could occur in the absence of MYC itself [2].

In order to test this hypothesis we analyzed the *MXI1-NUTM1* tumor for a MYC transcriptional signature [32]. We found a hallmark MYC target gene expression signature in both the *MXI1-NUTM1* tumor (normalized enrichment score 2.43, $p < 0.001$) and the *BRD3-NUTM1* NC (normalized enrichment score 2.64, $p < 0.001$) both with a false discovery rate (FDR) of <0.001 (Fig. 4b, c). MYC protein expression was undetectable by IHC in the *MXI1-NUTM1* tumor (Fig. 3d) and MYC transcripts in the normalized samples were ~23-fold less than in the *BRD3-NUTM1* NC, most consistent with a origin of the signature in the *MXI1-NUTM1* tumor from a non-MYC source. However, we had observed some MYC expression in some endothelial cells and stromal cells within the *MXI1-NUTM1* tumor by IHC, and in a sample comprised of benign esophageal wall adjacent to the tumor there was a MYC transcriptional signature (not shown). This raised the possibility that benign cells and not tumor cells were in part responsible for the MYC signature

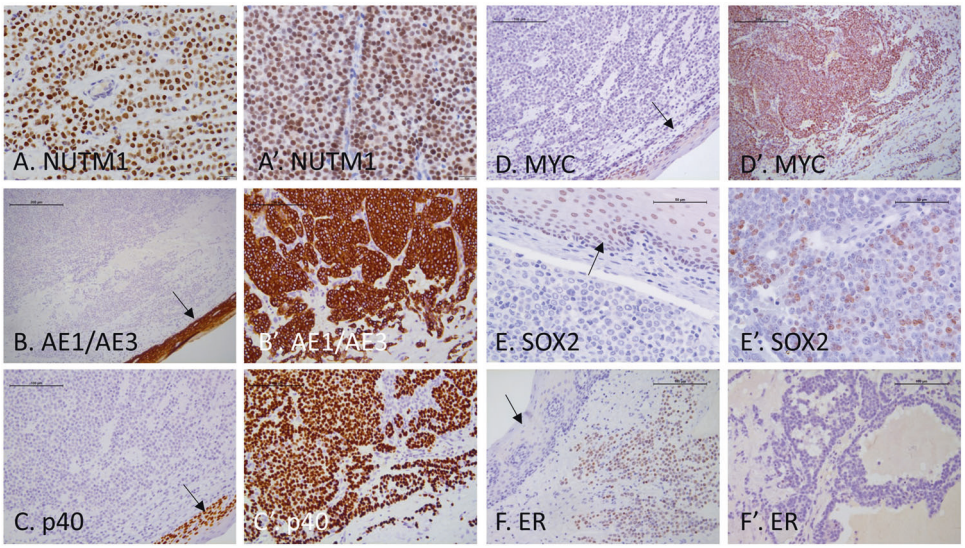

Fig. 3 Protein expression in the *MXI1-NUTM1* tumor and a *BRD3-NUTM1* carcinoma. Representative paired images of protein expression by IHC in the *MXI1-NUTM1* tumor (**a**–**f**) and a *BRD3-NUTM1* carcinoma (**a′**–**f′**). Both tumors express NUTM1. The *BRD3-NUTM1* carcinoma, but not the *MXI1-NUTM1* tumor, expresses pan-cytokeratin AE1/AE3, p40, MYC, and SOX2. The *MXI1-NUTM1* tumor, but not the *BRD3-NUTM1* carcinoma, weakly expresses ER. Arrows show benign esophageal squamous epithelium in the *MXI1-NUMT1* tumor expressing AE1/AE3, p40, MYC, and SOX2, but not ER.

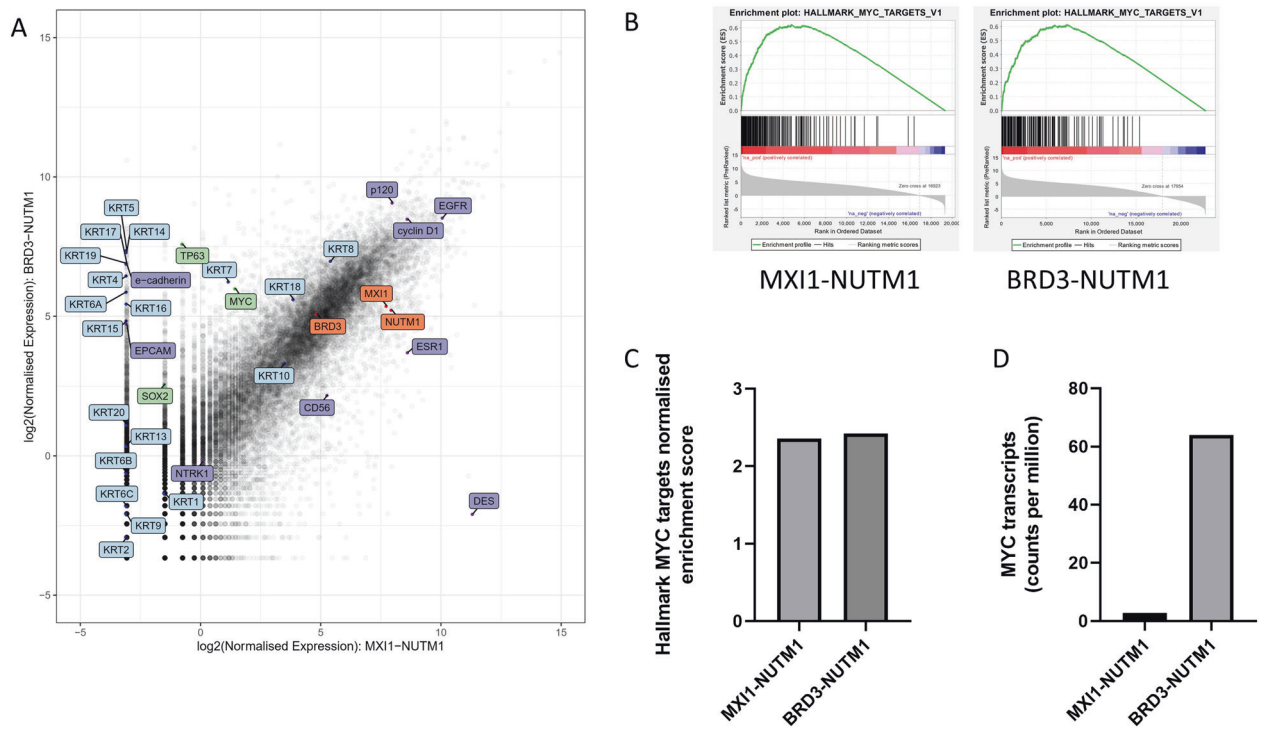

Fig. 4 Transcriptome analysis of the *MXI1-NUTM1* tumor and a *BRD3-NUTM1* carcinoma. a Scatterplot of normalized RNA expression. Genes known to be critical for oncogenesis in NC (*MYC*, *TP63* and *SOX2*) are labeled green, keratins blue, genes involved in the fusions orange, and other genes discussed in the main text and supplementary material purple. Hallmark MYC Targets v1 analysis (**b**) and normalized enrichment scores (**c**). **d** MYC transcript expression (normalized data, converted into base 10 from $\log_2$ data in Fig. 4**a**).

in the *MXI1-NUTM1* tumor sample. To control for this potential effect we performed comparative enrichment analysis based on log fold-change of *MXI1-NUTM1* tumor versus normal esophageal wall transcriptome data. We estimated tumor cell purity to be about 80% in the *MXI1-NUTM1* sample, but nevertheless if the MYC signature was

derived in part or even wholly from benign stromal cells then the FDR from a hallmark MYC target gene analysis of the comparison should not reach significance. In fact a MYC transcriptional signature was still readily detected in this comparison analysis (normalized enrichment score 3.79, $p < 0.001$, FDR < 0.001). This argues strongly that the *MXI1-NUTM1* tumor cells were the source of the MYC target signature.

MXI1-NUTM1 partially phenocopies the effect of MYC on cell proliferation and anchorage-independent growth in vitro

The contribution of MYC to oncogenesis is complex, but it has important and well-described roles in promoting cell proliferation and anchorage-independent growth in vitro. In order to determine if MXI1-NUTM1 also shared these MYC-type roles we transfected NIH-3T3 mouse fibroblasts with vectors constitutively expressing MXI1-NUTM1 and performed cell growth assays. We used MYC-expressing cells as a positive control. Expression of MXI1-NUTM1 and MYC was confirmed with immunoblots (Fig. 5a; the MXI1-NUTM1 was HA-tagged in order to facilitate its detection). In low serum (1%) conditions cell numbers were modestly but significantly increased in MXI1-NUTM1-expressing cells compared to empty vector (EV) controls as assessed by both ATP abundance (Cell Titer Glo assays) and Incucyte cell confluency assays (Fig. 5b, c). We noted similar, but greater increases in both ATP abundance and cell confluency in MYC-expressing cells (Fig. 5b, c). ATP concentrations fell rapidly after day 2 in MYC-expressing cells, probably due to exhaustion of nutrients.

MYC synergizes with activated RAS/MAPK pathway in rodent cells to produce anchorage-independent growth through suppression of senescence and apoptosis, key hallmarks of oncogenic transformation [33]. We performed soft agar colony formation assays in NIH-3T3 mouse fibroblasts cells to test if MXI1-NUTM1 could similarly cooperate with a constitutively active oncogenic HRAS (G12V) to promote anchorage independent growth. High levels of HRAS and pERK1/2 were confirmed in these cells (Fig. 5a and not shown). HRAS-expressing cells grew in aggregates that confounded the confluency assay, and were difficult to lyse, confounding the Cell Titer Glo assay. However, well-formed colonies grew in both adherent culture and semi-solid soft agar assays. Colony numbers were modestly but significantly increased in MXI1-NUTM1 + HRAS cells when compared with EV + HRAS control cells both on plastic (1.3-fold increase, $p = 0.0047$; Fig. 6a), and in the semi-solid soft agar assay (1.2-fold increase, $p = 0.0029$; Fig. 6b). Mean and total colony area were also significantly increased in the soft agar assays in MXI1-NUTM1 + HRAS cells (1.2-fold increase, $p = 0.0002$ and

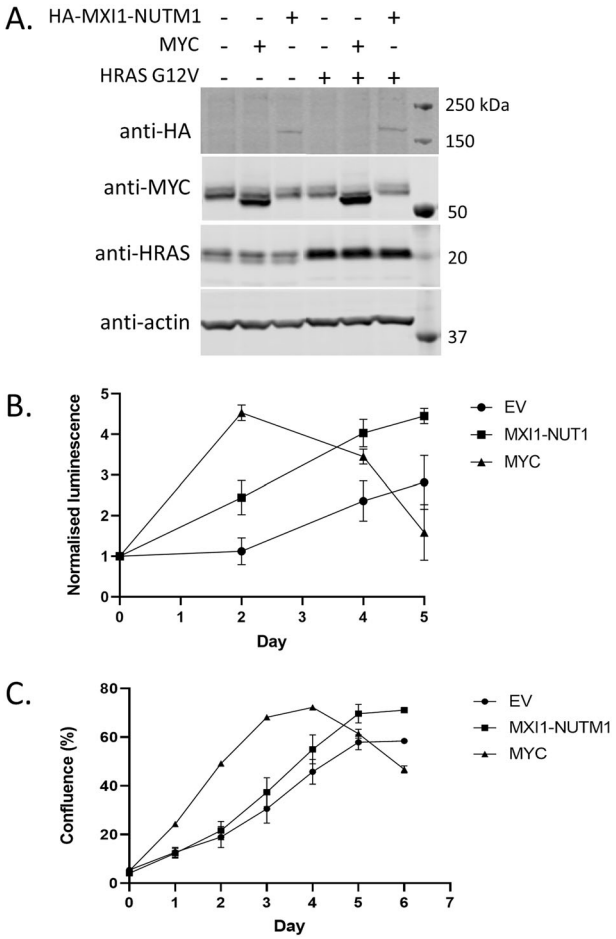

Fig. 5 MXI1-NUTM1 effect on cell proliferation in vitro. **a** Immunoblots with anti-hemagglutinin (HA), MYC, HRAS, and β-actin (loading control) antibodies on cell lysates from NIH-3T3 cells transduced with combinations of empty vector (EV), *HA-MXI1-NUTM1*, *MYC,* and oncogenic *HRAS* expressing retroviruses. A duplicate HA-MXI1-NUTM1-only lane has been cropped from the immunoblots for clarity. ATP abundance (**b** Cell Titer Glo assays) and cell confluency (**c** Incucyte assay) in NIH-3T3 cells transduced with either empty vector (EV), *HA-MXI1-NUTM1* or *MYC* (1% serum conditions). All data are expressed as the mean + SD.

1.4-fold $p < 0.0001$, respectively; Fig. 6b). As a positive control for these experiments we also overexpressed MYC together with oncogenic HRAS. This resulted in a 2.7-fold increase in the number of colonies grown on plastic ($p < 0.0001$, Fig. 6a). In the semi-solid soft agar assay MYC + HRAS increased colony numbers by 1.9-fold ($p < 0.0001$), mean colony area by 1.3-fold ($p < 0.0001$) and the total colony area by 2.6-fold ($p < 0.0001$) when compared with EV + HRAS control cells (Fig. 6b).

The apparently greater potency of MYC compared to MXI1-NUT did not appear to be due to increased cell proliferation or decreased apoptosis as assessed by Ki67 and cleaved caspase-3 labeling performed on cell blocks, respectively (not shown). In part, it was likely due to epigenetic silencing of the *MXI1-NUTM1* construct over time,

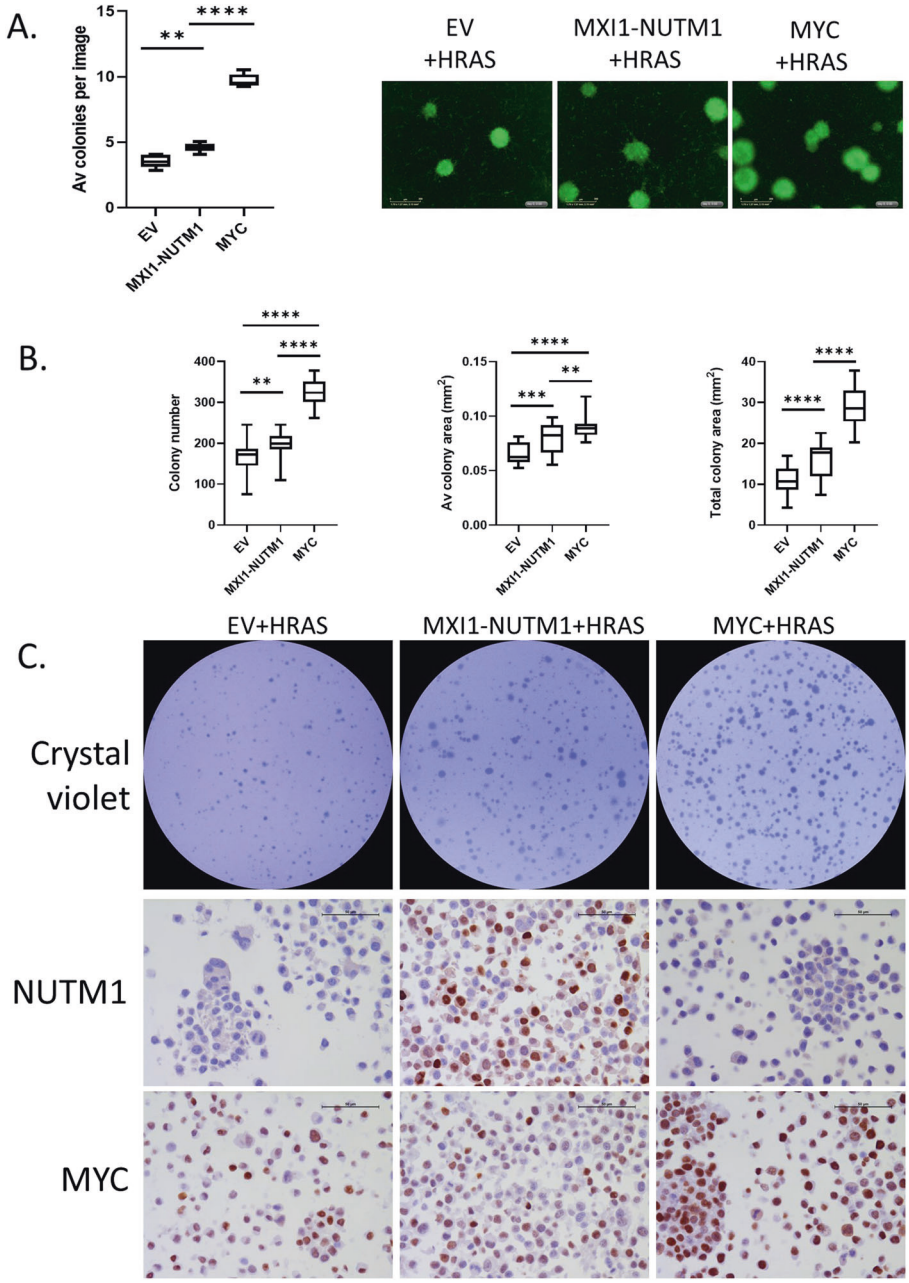

Fig. 6 MXI1-NUTM1 effect on anchorage-independent growth in vitro. NIH-3T3 cells transduced with oncogenic *HRAS* (from a *HRAS-IRES-GFP* vector) and either empty vector (EV), *HA-MXI1-NUTM1*, or *MYC*. **a** Cells grown on plastic substrate in 10% serum, showing box and whisker plots of colony number and representative images of colonies (visualized by GFP fluorescence). **b** Cells grown in soft agar, 10% serum. Box and whisker plots for colony number, area per colony and total colony area. **c** Images of colonies from cells grown in soft agar, 10% serum (top row) and IHC for NUTM1 and MYC on paraffin blocks of cells grown on plastic in 10% serum. Statistical comparisons were made using unpaired two-tailed *t*-tests. Data were analyzed using GraphPad Prism 8.1.0. $*p < 0.05$, $**p < 0.01$, $***p < 0.001$, $****p < 0.0001$.

as by immunoblot we observed a marked reduction of MXI1-NUTM1 protein expression with increasing passage number (not shown). IHC of cell blocks showed that only ~40% MXI1-NUTM1 + HRAS cells expressed detectable NUTM1, which could also explain why the effects of MXI1-NUTM1 were modest when compared to MYC (Fig. 6c). Unfortunately, we were unable to restore MXI1-NUTM1 expression by re-selection with antibiotics, and progressive silencing rendered further experiments untenable. Therefore, expression of MXI1-NUTM1 partially recapitulated the MYC-induced increase in proliferation and anchorage-independent growth in concert with oncogenic HRAS.

Discussion

MAD-NUTM1 tumors are probably best classified as sarcomas. They have been reported in soft tissue as well as viscera [3] and can metastasize to lymph nodes and lung. The *MXI1-NUTM1* tumor described here showed similar features to previously described *MAD-NUTM1* tumors, with small round cells and rhabdoid cell morphology, and no specific differentiation lineage by IHC and transcriptome profiling. NCs also have a primitive small round cell component, but in contrast to *MAD-NUTM1* tumors they typically show small foci of squamous differentiation.

These foci may be infrequent and therefore not be identified in small biopsies. The *MXI1-NUTM1* tumor did not express typical markers of NCs including cytokeratins and p40 (ΔNp63). For example, a recent paper documented expression of cytokeratins or p40/p63 in 17 of 19 NCs [5]. Furthermore, oncogenic drivers of NCs, including MYC, TP63, and SOX2 [28–30], were not expressed in the *MXI1-NUTM1* tumor. MYC, TP63, and SOX2 provide a direct link between the BRD-NUTM1 fusion and the oncogenic mechanism in NCs. They map to chromatin megadomains that are hyperacetylated and transcriptionally activated by BRD4-NUTM1. RNAi knockdown of any one of these genes blocks cell proliferation in NC cell lines, and in the case of *MYC* and *SOX2*, also induces differentiation [28–30].

The absence of MYC, TP63, and SOX2, together with the functional disparity between BRD and MAD proteins, argues for a different oncogenic mechanism for *MAD-NUTM1* fusions compared with *BRD-NUTM1* fusions. Previously we have suggested that the fusion of NUTM1 to the C-terminal region of a MAD family protein could potentially convert it from a repressor to an activator of MYC target genes [2]. MAD proteins compete with MYC for binding to MYC-Associated Factor X (MAX). MYC/MAX heterodimers bind to sequences in promoters known as E-boxes and increase gene expression through transcriptional elongation, whereas MAD/MAX heterodimers bind E-boxes but inhibit transcription through mSin3 and histone deacetylases [34, 35]. The set of MYC responsive genes can alter depending on the cellular context, but they have important roles in cell cycle, cell growth, apoptosis and cellular metabolism, amongst others. Therefore, competition between MYC and MAD for binding to MAX has a major impact on many "hallmarks of cancer" processes. Our hypothesis is that since the MAD portion of MAD-NUTM1 fusions retain their basic region/helix-loop-helix/leucine zipper domains they would be capable of heterodimerizing with MAX and binding E-boxes. However, unlike wild-type MAD, they would also recruit the histone acetyltransferase p300 through the AD1 domain of NUTM1 and cause transcriptional activation of MYC target genes [2]. Here we provide support for this model by demonstrating a similar transcriptome-wide enrichment of MYC target genes in the *MXI1-NUTM1* tumor and a NC, despite the absence of MYC expression in the former. We also show that the MXI1-NUTM1 fusion can at least partly phenocopy the effect of MYC on cell proliferation and anchorage-independent growth in vitro, which to the best of our knowledge is the first experimental demonstration of an oncogenic mechanism for a MAD-NUTM1 protein.

We stress that our model for the oncogenic mechanism of *MAD-NUTM1* fusions remains speculative. Analysis of other tumors with *MAD-NUTM1* fusions and mechanistic studies on their chimeric proteins are required to confirm the key features including binding to MAX and E-box motifs in MYC target genes. Furthermore, it was evident that MXI1-NUTM1 was not as potent as MYC in our in vitro assays. This may be partially due to the use of a fibroblast cell line, but was clearly also due to silencing of the integrated *MXI1-NUTM1* construct. At the time of our colony assays, only about 40% of the *MXI1-NUTM1* transformed cells continued to express NUTM1. Stable cell lines expressing recombinant *BRD4-NUTM1* have yet to be created [29], suggesting that it may be similarly difficult to create stable cell lines expressing *MAD-NUTM1*, in which case either cultured primary tumor cells or inducible cell lines may be required for thorough mechanistic analyses.

This work raises the likelihood that *NUTM1*-fusions from other NRNs also have different oncogenic mechanisms to *BRD-NUTM1* fusions. NRNs are increasingly being viewed as several distinct subgroups, and we have recently argued that their classification, clinical behavior, and therapeutic options may be best defined by the *NUTM1* fusion partner, rather than by tumor morphology or IHC profile [2]. Although there are some promising results from the treatment of NCs with BET inhibitors [36, 37], it would follow that BET inhibitors may be ineffective against NRNs that lack the bromodomain-histone acetylated chromatin feed forward mechanism seen in NCs. Consistent with this, some non-NC NRNs respond to standard therapies for their tumor group.

MAD-NUTM1 tumors and other NRNs illustrate that there are important diagnostic and potentially therapeutic implications if a diagnosis of NC is incorrectly made based on a positive NUTM1 IHC or FISH alone. We suggest that in addition to the liberal use of NUTM1 IHC as a relatively cheap and sensitive screen for NRNs, all NUTM1 IHC-positive cases should be rigorously assessed for evidence of epithelial and squamous differentiation by morphology and IHC prior to making a diagnosis of NC. Ideally, confirmatory molecular testing should also be performed in order to identify the *NUTM1* fusion partner for diagnostic certainty. In this regard RNA sequencing appears to be more sensitive than DNA intron tiling sequencing. We readily detected the *MXI1-NUTM1* fusion with multiple RNA sequencing technologies but failed with a DNA targeted panel approach, most likely because the *NUTM1* intron where the breakpoint occurred (intron 2) contains several regions of low complexity DNA sequence. In summary, the novel *MXI1-NUTM1* fusion that we describe here illustrates how a diagnostic approach that integrates morphological, immunohistochemical and molecular data can be critical to inform appropriate clinical management, as well as reveal novel biological mechanisms.

Acknowledgements The authors wish to acknowledge Tim Semple, David Yoannidis, and Gisela Mir Arnau for performing RNAseq, and Anna Korczynski for technical assistance. Tumor profiling at Peter Mac is made possible by the generous support of the Peter MacCallum Foundation. SBF is funded by an NHMRC Practitioner Fellowship APP1079329.

Compliance with ethical standards

Conflict of interest The authors declare that they have no conflict of interest.

Publisher's note Springer Nature remains neutral with regard to jurisdictional claims in published maps and institutional affiliations.

References

1. French CA. NUT carcinoma: clinicopathologic features, pathogenesis, and treatment. Pathol Int. 2018;68:583–95.
2. McEvoy CR, Fox SB, Prall OWJ. Emerging entities in NUTM1-rearranged neoplasms. Genes Chromosomes Cancer. 2020;59:375–85.
3. Dickson BC, Sung YS, Rosenblum MK, Reuter VE, Harb M, Wunder JS, et al. NUTM1 gene fusions characterize a subset of undifferentiated soft tissue and visceral tumors. Am J Surg Pathol. 2018;42:636–45.
4. Tamura R, Nakaoka H, Yoshihara K, Mori Y, Yachida N, Nishikawa N, et al. Novel MXD4-NUTM1 fusion transcript identified in primary ovarian undifferentiated small round cell sarcoma. Genes Chromosomes Cancer. 2018;57:557–63.
5. Stevens TM, Morlote D, Xiu J, Swensen J, Brandwein-Weber M, Miettinen MM, et al. NUTM1-rearranged neoplasia: a multi-institution experience yields novel fusion partners and expands the histologic spectrum. Mod Pathol. 2019;32:764–73.
6. Diolaiti D, Dela Cruz FS, Gundem G, Bouvier N, Boulad M, Zhang Y, et al. A recurrent novel MGA-NUTM1 fusion identifies a new subtype of high-grade spindle cell sarcoma. Cold Spring Harb Mol Case Stud. 2018;4:a003194.
7. Mantilla JG, Ricciotti RW, Chen E, Hoch BL, Liu YJ. Detecting disease-defining gene fusions in unclassified round cell sarcomas using anchored multiplex PCR/targeted RNA next-generation sequencing-molecular and clinicopathological characterization of 16 cases. Genes Chromosomes Cancer. 2019;58:713–22.
8. Goto T, Arai Y, Shibata T, Oyama T, Yoshida A. Sarcoma with MGA-NUTM1 fusion in the lung: an emerging entity. Virchows Arch. 2020;476:317–22.
9. Zheng Z, Liebers M, Zhelyazkova B, Cao Y, Panditi D, Lynch KD, et al. Anchored multiplex PCR for targeted next-generation sequencing. Nat Med. 2014;20:1479–84.
10. McEvoy CR, Semple T, Yellapu B, Choong DY, Xu H, Mir Arnau G, et al. Improved next-generation sequencing pre-capture library yields and sequencing parameters using on-bead PCR. Biotechniques. 2020;68:48–51.
11. Koboldt DC, Chen K, Wylie T, Larson DE, McLellan MD, Mardis ER, et al. VarScan: variant detection in massively parallel sequencing of individual and pooled samples. Bioinformatics. 2009;25:2283–5.
12. Cibulskis K, Lawrence MS, Carter SL, Sivachenko A, Jaffe D, Sougnez C, et al. Sensitive detection of somatic point mutations in impure and heterogeneous cancer samples. Nat Biotechnol. 2013;31:213–9.
13. Rosenthal R, McGranahan N, Herrero J, Taylor BS, Swanton C. DeconstructSigs: delineating mutational processes in single tumors distinguishes DNA repair deficiencies and patterns of carcinoma evolution. Genome Biol. 2016;17:31.
14. Markham JF, Yerneni S, Ryland GL, Leong HS, Fellowes A, Thompson ER, et al. CNspector: a web-based tool for visualisation and clinical diagnosis of copy number variation from next generation sequencing. Sci Rep. 2019;9:6426.
15. Martin M. Cutadapt removes adapter sequences from high-throughput sequencing reads. EMBnet J. 2011;17:10–2.
16. Pertea M, Kim D, Pertea GM, Leek JT, Salzberg SL. Transcript-level expression analysis of RNA-seq experiments with HISAT, StringTie and Ballgown. Nat Protoc. 2016;11:1650–67.
17. Anders S, Pyl PT, Huber W. HTSeq–a Python framework to work with high-throughput sequencing data. Bioinformatics. 2015;31:166–9.
18. Law CW, Chen Y, Shi W, Smyth GK. voom: precision weights unlock linear model analysis tools for RNA-seq read counts. Genome Biol. 2014;15:R29.
19. Davidson NM, Majewski IJ, Oshlack A. JAFFA: high sensitivity transcriptome-focused fusion gene detection. Genome Med. 2015;7:43.
20. Uhrig S. Arriba—Fast and accurate gene fusion detection from RNA-Seq data. https://github.com/suhrig/arriba. 2019.
21. Subramanian A, Tamayo P, Mootha VK, Mukherjee S, Ebert BL, Gillette MA, et al. Gene set enrichment analysis: a knowledge-based approach for interpreting genome-wide expression profiles. Proc Natl Acad Sci USA. 2005;102:15545–50.
22. Patro R, Duggal G, Love MI, Irizarry RA, Kingsford C. Salmon provides fast and bias-aware quantification of transcript expression. Nat Methods. 2017;14:417–9.
23. Swarbrick A, Roy E, Allen T, Bishop JM. Id1 cooperates with oncogenic Ras to induce metastatic mammary carcinoma by subversion of the cellular senescence response. Proc Natl Acad Sci USA. 2008;105:5402–7.
24. Du F, Zhao X, Fan D. Soft agar colony formation assay as a hallmark of carcinogenesis. Bio-protocol. 2017;7:e2351.
25. Law AMK, Yin JXM, Castillo L, Young AIJ, Piggin C, Rogers S, et al. Andy's Algorithms: new automated digital image analysis pipelines for FIJI. Sci Rep. 2017;7:15717.
26. Reynoird N, Schwartz BE, Delvecchio M, Sadoul K, Meyers D, Mukherjee C, et al. Oncogenesis by sequestration of CBP/p300 in transcriptionally inactive hyperacetylated chromatin domains. EMBO J. 2010;29:2943–52.
27. Haack H, Johnson LA, Fry CJ, Crosby K, Polakiewicz RD, Stelow EB, et al. Diagnosis of NUT midline carcinoma using a NUT-specific monoclonal antibody. Am J Surg Pathol. 2009;33:984–91.
28. Grayson AR, Walsh EM, Cameron MJ, Godec J, Ashworth T, Ambrose JM, et al. MYC, a downstream target of BRD-NUT, is necessary and sufficient for the blockade of differentiation in NUT midline carcinoma. Oncogene. 2014;33:1736–42.
29. Alekseyenko AA, Walsh EM, Wang X, Grayson AR, Hsi PT, Kharchenko PV, et al. The oncogenic BRD4-NUT chromatin regulator drives aberrant transcription within large topological domains. Genes Dev. 2015;29:1507–23.
30. Wang R, Liu W, Helfer CM, Bradner JE, Hornick JL, Janicki SM, et al. Activation of SOX2 expression by BRD4-NUT oncogenic fusion drives neoplastic transformation in NUT midline carcinoma. Cancer Res. 2014;74:3332–43.
31. French C. NUT midline carcinoma. Nat Rev Cancer. 2014;14:149–50.
32. Liberzon A, Birger C, Thorvaldsdottir H, Ghandi M, Mesirov JP, Tamayo P. The Molecular Signatures Database (MSigDB) hallmark gene set collection. Cell Syst. 2015;1:417–25.
33. Hanahan D, Weinberg RA. The hallmarks of cancer. Cell. 2000;100:57–70.

34. Schreiber-Agus N, DePinho RA. Repression by the Mad(Mxi1)-Sin3 complex. Bioessays. 1998;20:808–18.
35. Luscher B, Vervoorts J. Regulation of gene transcription by the oncoprotein MYC. Gene. 2012;494:145–60.
36. Stathis A, Zucca E, Bekradda M, Gomez-Roca C, Delord JP, de La Motte Rouge T, et al. Clinical response of carcinomas harboring the BRD4-NUT oncoprotein to the targeted bromodomain inhibitor OTX015/MK-8628. Cancer Discov. 2016;6:492–500.
37. Lewin J, Soria JC, Stathis A, Delord JP, Peters S, Awada A, et al. Phase Ib trial with birabresib, a small-molecule inhibitor of bromodomain and extraterminal proteins, in patients with selected advanced solid tumors. J Clin Oncol. 2018;36:3007–14.